Dynamics of wave-supported gravity currents in intermediate water

Marino, Massimiliano; Stagnitti, Martina; Stancanelli, Laura Maria; Musumeci, Rosaria Ester; Foti, Enrico

DOI
10.1016/j.csr.2023.105082

Publication date
2023

Document Version
Final published version

Published in
Continental Shelf Research

Citation (APA)
Marino, M., Stagnitti, M., Stancanelli, L. M., Musumeci, R. E., & Foti, E. (2023). Dynamics of wave-supported gravity currents in intermediate water. *Continental Shelf Research*, *267*, Article 105082. https://doi.org/10.1016/j.csr.2023.105082

Continental Shelf Research 267 (2023) 105082

Contents lists available at ScienceDirect

Continental Shelf Research

journal homepage: www.elsevier.com/locate/csr

Research papers

Dynamics of wave-supported gravity currents in intermediate water

Massimiliano Marino [a,*], Martina Stagnitti [a], Laura Maria Stancanelli [b], Rosaria Ester Musumeci [a], Enrico Foti [a]

[a] Department of Civil Engineering and Architecture, University of Catania, Via Santa Sofia 64, Catania, 95123, Italy
[b] TU Delft, Department of Hydraulic Engineering, Delft University of Technology, Stevinweg 1, 2628 CN, Delft, The Netherlands

ARTICLE INFO

Keywords:
Density currents
Point-release setup
Physical modeling

ABSTRACT

The dynamics of gravity currents propagating beneath intermediate water waves is investigated in the present study. Laboratory experiments were carried out in a wave flume, in which saltwater was released into freshwater by means of a point-release setup in the presence of a fully developed wave field. Results revealed a series of interesting features of the gravity current advancement and density distribution under the influence of the wave field. The advancing fronts oscillate with the same period of the wave, although front velocity appears not to be affected by increasing wave nonlinearity. The analysis of the density field highlighted the existence of an enhanced mixing process between ambient and gravity current fluid induced by the orbital motion, alongside a loss of symmetry between onshore and offshore fronts, in terms of front shape and density spatial distribution. Such an effect intensifies as wave height increases and wavelength decreases. Moreover, variations of the salinity concentration profiles during the wave phase revealed a "piston-type" oscillatory behavior of the gravity current concentration induced by the wave field, which oscillates accordingly to the wave phase.

1. Introduction

Gravity currents are common physical processes in coastal areas. They can be generated by natural density gradients, such as salt wedges and turbidity currents, or by anthropic activities, which include dredging, oil spill, desalination processes etc. Parker et al. (1987), Fannelop and Waldman (1972), Stancanelli et al. (2017), Ben Meftah et al. (2018). The presence of such flows have significant consequences on coastal sediment transport and heavily influence migration, production and diversity of benthic organisms (Bigham et al., 2020).

In the nearshore, the dynamics of gravity currents is heavily influenced by the presence of waves. This is particularly important in intermediate waters, where leaks from vessels can reach the seabed and the pollutant hydrodynamics is influenced by the wave motion field all along the water column. However, the vast majority of existing efforts investigated gravity currents propagating in quiescent ambient fluids, within horizontal smooth beds (Rottman and Simpson, 1983; Nogueira et al., 2014; Ottolenghi et al., 2016; Longo et al., 2018; Pelmard et al., 2021; Kokkinos and Prinos, 2022), rough beds (Cenedese and Dalziel, 1998; Nogueira et al., 2013a; Han et al., 2021; Maggi et al., 2022) porous beds (Venuleo et al., 2019), sloping beds (Lombardi et al., 2015; Ho and Lin, 2015; He et al., 2018; Dai and Huang, 2020, 2021; De Falco et al., 2020; Maggi et al., 2023a,b), in the presence of obstacles (Gonzalez-Juez et al., 2009; Tokyay et al., 2014; De Falco et al., 2021b) and within rotating frames (Negretti et al., 2021; De Falco et al., 2021a; Wirth and Negretti, 2022).

Studies on gravity current-surface waves interaction are indeed very limited. Ng and Fu (2002) developed an asymptotic theory for the propagation of a layer of viscous dense fluid beneath surface waves. Evolution equations to model the profile distribution of the viscous fluid are obtained. The authors found that the streaming current generated by the oscillatory flow generally dominates inducing the density current to advance together the waves.

Robinson et al. (2013) investigated the interaction of waves with the dynamics of the density current propagation under different wave regimes. A volume of dense fluid was point-released into a water wave field, which generated a two-front gravity current. Two opposite observations were reported. In the presence of short waves, the gravity current was advected in the opposite direction of the waves. Whereas, in the presence of long waves, the Stokes drift close the bed dominated and the current was transported in the wave direction. Moreover, results reported an asymmetry of the downstream and upstream gravity current heads.

Laboratory investigations on gravity currents in the presence of waves were carried out by Musumeci et al. (2017) and Stancanelli et al.

* Corresponding author.
E-mail address: massimiliano.marino@unict.it (M. Marino).

https://doi.org/10.1016/j.csr.2023.105082
Received 8 November 2022; Received in revised form 26 April 2023; Accepted 26 July 2023
Available online 29 July 2023

(2018b). In intermediate waters, they found that the front propagation during the initial stage (known as slumping) is characterized by a constant velocity, and that the front propagates with a pulsating behavior with the same period of the wave.

Viviano et al. (2018) investigated turbulence related quantities in a wave-gravity current field by means of a numerical model. The model couples a Boussinesq-type model and density current model for stratified flows. Subgrid turbulence is included by means of two turbulence closure models. The model was validated by means of experimental data. Results showed that, in the presence of surface waves, a reduction of turbulence production occur, alongside an increment of the mixing of the dense and the ambient fluid. Analogously, Stancanelli et al. (2018a) investigated the dynamics of the density currents in the presence of waves by means of a CFD model, showing that Large Eddy Simulations can more realistically model turbulent processes such as formation of interfacial Kelvin–Helmholtz billows and vortex stretching than other two-equations turbulence closures.

Recently, Cui et al. (2022) investigated gravity flows in the presence of surface waves using a numerical model with Large Eddy Simulation to model sub-grid turbulent flow. The results showed that the period of the front oscillation is correlated to the period of the surface wave, and that the amplitude of the oscillation increases with wave height. Moreover, wave motion influences the arising position and coherent direction of the turbulent structures in the pycnocline. Oscillating wave motion stabilizes pycnocline earlier and hamper turbulent mixing. The instability region decreases faster with higher wave height, but not with longer wavelength.

Notwithstanding previous research efforts, several questions regarding interaction between waves and gravity currents remain unanswered. One essential aspect to investigate is the salinity concentration distribution along the vertical profile, which can provide insights into potential detrimental effects on marine seabed biota, which may be exacerbated by the presence of waves. In addition, adopting a wider range of density difference could extend the knowledge on the propagation dynamics, discerning whether the phenomenon is dominated by the wave field or by the density difference. Furthermore, investigating the influence of wave asymmetry can provide insights on how the skewed distribution of the wave velocity field could potentially influence gravity current hydrodynamics.

The present paper illustrates a novel experimental study on the interaction of gravity currents and waves by means of a laboratory investigation. The goal of the study is to characterize the onshore and offshore propagation of gravity current by studying the current velocity and density field. A high-resolution camera is employed to track the front advancement, from which concentration maps and vertical profiles were obtained. Concentration maps allowed to track the dynamics of the current density field and characterize the internal hydrodynamics of the current.

The device used to generate the gravity current is a point-release setup. Such a device, which was employed very rarely in the study of waves-gravity current interaction (Chowdhury and Testik, 2014), is well suited to simulate leakages and vertical outfall in the sea. Moreover, it allows the generation of two fronts and therefore to investigate the propagation of the density current in the same and the opposite directions of the waves simultaneously.

Effects of the density difference between gravity current and ambient fluid, which were rarely studied in previous studies, are herein investigated by means of a wide range of experimented current fluid densities. Moreover, a focus is given to the effects of wave nonlinearity on the propagation of the gravity current front. The generation of a fully developed wave field allowed to investigate the influence of second-order effects (i.e. Stokes drift) and steady streaming. Finally, the vertical density variation is analyzed during the different phases of the wave period, in order to investigate gravity current-ambient fluid mixing induced by the orbital motion.

The paper is organized as follows. Section 2 describes the experimental apparatus, the experiments plan and the data analysis methodology. A preliminary characterization of the ambient fluid velocity field in the absence of the gravity current is discussed in Section 3. The experimental evidences are presented and analyzed in Section 4, in terms of the gravity current front propagation (see Section 4.1) and of the current concentration evolution (see Section 4.2). Conclusion and final remarks are given in Section 5.

2. Experiments and methods

The experiments were carried out in a hydraulic channel 9.00 m long, 0.50 m wide and 0.70 m deep (Fig. 1), equipped with a piston-type wave-maker at one end and an absorbing beach at the other end. The free-surface wave elevation was measured with four acoustic probes produced by Pepperl+Fuchs model UC500-30GM70-IE2R2-V15. The horizontal and vertical components of the wave-induced velocity field were measured by means of an Acoustic Doppler Velocimeter manufactured by Nortek model Vectrino Profiler, with an acquisition frequency of 50 Hz.

A reservoir, connected to a small pipe having diameter equal to 0.01 m, whose outlet is located at the free surface, is placed above the flume at 6.00 m from the wave-maker. The gravity current is generated by releasing a finite volume of saltwater, having density ρ_1, in the flume which is filled with fresh water, having density $\rho_2 < \rho_1$. Fig. 2 shows a sketch of the device used for the point release of the density current, where x_{on} and x_{off} are the onshore-directed and the offshore-directed front positions.

Sodium chlorate was used in all the experiments to obtain saltwater of a fixed density. Green food dye was then added to the saltwater solution to make the density current visible. The concentration of the diluted dye is about 0.6%. The molecular diffusivity of the dye in water is O(10^{-6} cm^2/s) while that of the saltwater is O(10^{-4} cm^2/s). Therefore, the differential diffusion between the dye and the salt water are assumed negligible (Stancanelli et al., 2018b). Density of saltwater and freshwater were measured by a procedure that allows the measurement of the density of solutions through the comparison with a fluid of known density, in our case distilled water. Accuracy of the measured density is 1 g/m^3. The solutions were placed in 100-ml pycnometers and, by means of a series of weighings, a density ratio between the solution under analysis and a solution of known density can be obtained using the following formula:

$$\delta = \frac{m_2 - m_1'}{m_3 - m_1} = \frac{\rho_s}{\rho} \tag{1}$$

where m_2 is the weight of the pycnometer with the solution, m_3 is the weight of the pycnometer with distilled water, m_1' is the weight of the empty pycnometer before weighing with distilled water, and m_1 is the weight of the empty pycnometer before weighing with the saline solution. The computed δ is equal to the ratio between the densities ρ_s/ρ, where ρ_s is the density of the solution and ρ is the known density of distilled water.

For each test, a volume V_r of dye-saltwater solution equal to 200 ml is released in the wave flume with water depth h equal to 0.20 m. The gravity current formation and expansion is investigated considering the following hydraulic regimes: (i) initially quiescent ambient fluid; (ii) presence of regular surface waves. In the second case, in order to run the experiment in a completely developed regular wave field, the release is carried out after 1 h from the activation of the wave-maker. For both hydraulic regimes, after the initial collapse of the fluid to the bottom, the gravity current propagates horizontally beneath the lighter fluid in two opposite directions, as showed in Fig. 2. The propagation of the two fronts was recorded by means of a Sony HDR-CX410VE HD camera (frame rate of 25 FPS). The measuring area extends 0.80 m in the horizontal direction, with the middle section located 6.00 m far from the wave-maker, which corresponds to the release point.

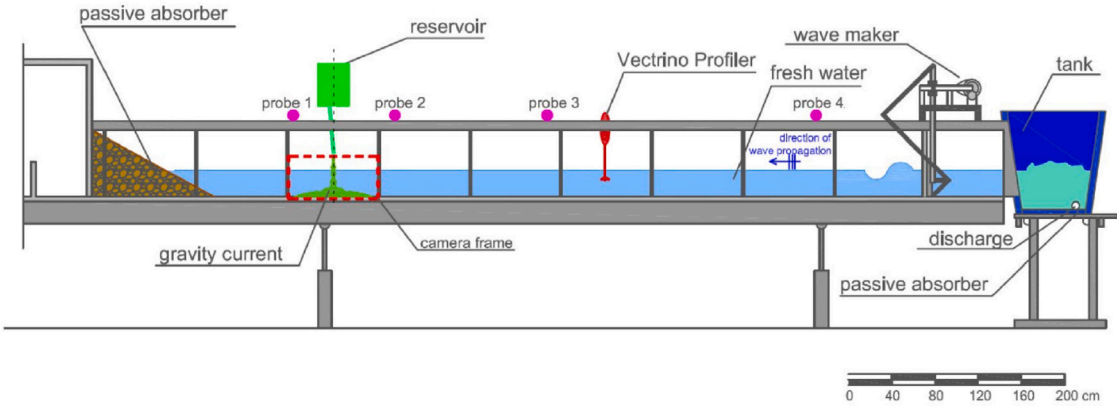

Fig. 1. Sketch of the experimental apparatus of the point release tests, used both in the absence and in the presence of waves.

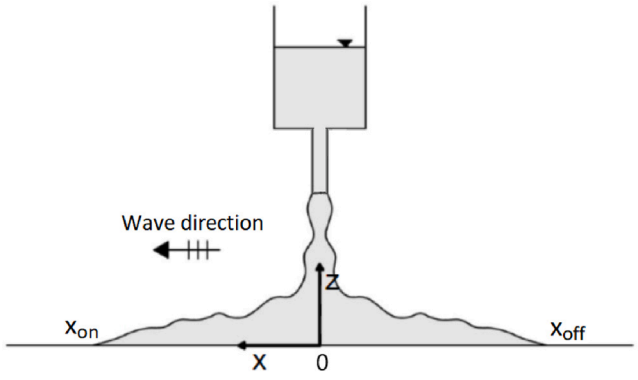

Fig. 2. Density current release device and adopted reference system.

Table 1
Control parameters of the experiments: ρ_1 and ρ_2 are the density of saltwater and fresh water respectively, g' is the reduced gravity, H is the wave height, T is the wave period, L is the wave length and H/L is the wave steepness. All the tests were performed with $h = 0.20$ m and $V_r = 200$ ml.

Test	ρ_1 [kg/m^3]	ρ_2 [kg/m^3]	g' [m/s^2]	H [m]	T [s]	L [m]	H/L
1	1,012.75	999.97	0.13	–	–	–	–
2	1,012.75	999.97	0.13	0.012	1.3	2.166	0.006
3	1,012.75	999.97	0.13	0.021	1.0	1.464	0.014
4	1,012.75	999.97	0.13	0.022	0.8	0.987	0.022
5	1,038.56	998.96	0.39	–	–	–	–
6	1,038.56	998.96	0.39	0.013	1.3	2.166	0.006
7	1,038.56	998.96	0.39	0.018	1.0	1.464	0.012
8	1,038.56	998.96	0.39	0.023	0.8	0.987	0.023
9	1,058.50	997.34	0.60	–	–	–	–
10	1,058.50	997.34	0.60	0.015	1.3	2.166	0.007
11	1,058.50	997.34	0.60	0.023	1.0	1.464	0.016
12	1,058.50	997.34	0.60	0.029	0.8	0.987	0.029

A series of 12 experimental tests was carried out. Table 1 reports the main control parameters of the experiments, i.e. the saltwater density ρ_1, the fresh water density ρ_2, the reduced gravity g', the wave height H, the wave period T, the wave length L calculated with the dispersion relationship, and the wave steepness H/L. The reduced gravity is determined as $g' = g(\rho_1 - \rho_2)/\rho_2$, where g is the gravitational acceleration. The experiments were carried out by considering a reduced gravity that ranges in the interval $0.13 \div 0.60$ m/s^2 and quiescent and three intermediate water wave regimes (i.e. $h/L = 0.1 \div 0.2$).

The gravity current diagnostics were carried out by applying standard image processing tools to determine the two fronts position and density concentration maps. In particular, the two fronts advancement with respect to the current center (see reference system in Fig. 2) was measured after converting the acquired RGB images into binary format, where the gravity current is a black-filled contour over a white background. In particular, the advancement of the gravity current fronts was measured with reference to the lower line of pixels, which corresponds to the bottom of the flume.

The gravity current mixing intruding into an ambient fluid characterized by less density is investigated through the analysis of density concentration distributions. In particular, the density concentration maps were obtained adopting the pixel intensity strategy (Nogueira et al., 2013b; Adduce et al., 2022). The maps were constructed from the reduction of the background light of the grey scale images caused by the advancing density current with respect to initial condition before the saltwater release, assuming a linear relationship between dye and salt concentration within the gravity current. The experimental setup was purposely designed in terms of illumination conditions, camera specifics and amount of color dye, in order to allow the acquisition of concentration measurements accurate enough with respect to density of the generated gravity currents, the size of the study area and the characteristic of the reproduced waves. The spatial resolution of the pixel intensity field, which is 1 pixel per mm, is suitable for the size of our rectangular study area (i.e. 0.800 × 0.200 m) and for the tested wave conditions (i.e. H in the range 0.012–0.029 m and L in the range 0.987–2.166 m). In particular, the intensity of 800 and 200 pixels in the horizontal and vertical directions were acquired, respectively, for a total of 160,000 pixels. Moreover, the wave-induced spatial variability of the pixel intensity was captured, being the spatial resolution one order of magnitude lower than the reproduced H. The homogeneity of the conversion from pixel intensity to density concentration over the whole study area was ensured by the spatially uniform brightness. In any case, assuming that brightness conditions do not change during the single experiment, the effects of any slight brightness non-uniformity would be removed by the subtraction of the background from each image corresponding to the considered time intervals.

For each test, the evolution of the density spatial distribution over time is represented through contour plots of the relative concentration C recovered for specific times, where $C = (\tilde{\rho} - \rho_2)/(\rho_1 - \rho_2)$ with $\tilde{\rho}$ being the fluid density at a generic x and z. Moreover, relative concentration profiles were calculated for different instants, considering reference vertical axes for both the onshore and offshore fronts.

3. Hydrodynamics of the ambient fluid

An analysis of the flow conditions in the presence of only surface waves is presented. As a measure of wave nonlinearity, the parameter a/h is computed, where $a = H/2$ is the wave amplitude. Wave nonlinearity of all tests lies in the range of $0.044 \div 0.195$. Reflection coefficients in the flume, which are obtained by means of Mansard and Funke (1980) three-probes method and Faraci et al. (2014) four-probes

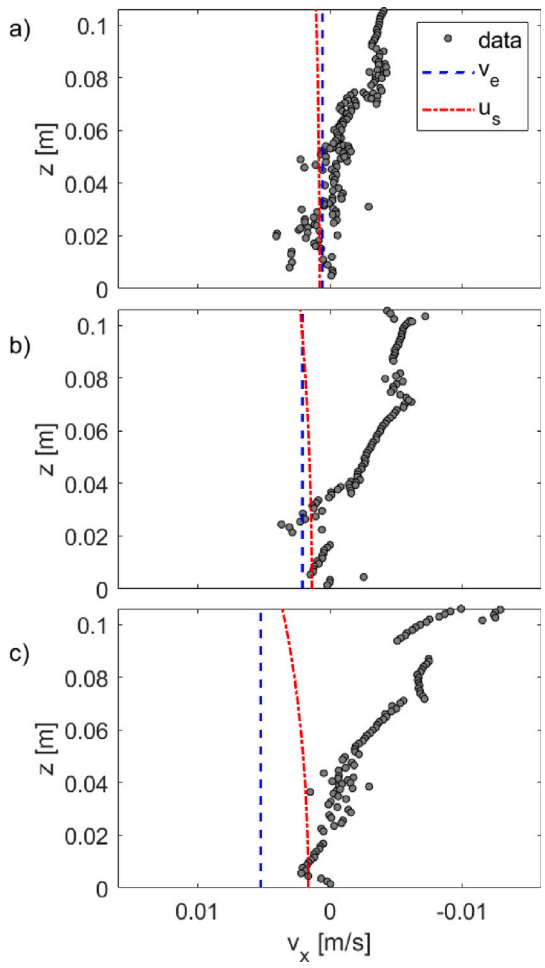

Fig. 3. Measured time-averaged velocity profiles over the water column acquired after the wave motion is completely developed (1 h of waves). Different wave regimes: (a) H = 0.015 m, T = 1.3 s; (b) H = 0.023 m, T = 1.0 s; (c) H = 0.029 m, T = 0.8 s. The Stokes drift velocity u_s along the water column and the Eulerian horizontal velocity between trough and wave crest v_e along the water depth as reference are reported.

method, are in the range of 0.10 ÷ 0.14 for both methods, showing that wave reflection is negligible.

Fig. 3 shows the wave-induced mean velocity profiles acquired by a Vectrino Profiler 1 h after starting the wave-maker in the absence of the gravity current, for three investigated wave conditions: (i) H = 0.015 m, T = 1.3 s (Fig. 3a); (ii) H = 0.023 m, T = 1.0 s (Fig. 3b); (iii) H = 0.029 m, T = 0.8 s (Fig. 3c). Fig. 3 reports also the computed Stokes drift velocity u_s along the water column and the Eulerian horizontal velocity between trough and wave crest v_e. The velocity measurements was confined to the vertical distance of 0 to 0.1 m. This is intended to delineate the flow characteristics within the gravitational current front propagation region, which in this study extends approximately from 0 to 0.05 m. This range allows for a comprehensive examination of the propagation zone and facilitates a detailed observation of the interfacial flow dynamics between the denser and ambient fluids.

A steady flow in the wave direction is observed at the bottom boundary layer for all three considered conditions, as a consequence of the fully developed wave field inside the flume. Indeed, the oscillatory flow generates both an orbital motion and a steady current. The latter can be considered as the sum of the Stokes drift, which is caused by the irrotational oscillatory motion, and the viscous steady streaming, which is determined by the vorticity generated at the boundary. It should be noted that the first component develops immediately, whereas the development of the second one depends on the channel length. In the present case the steady streaming takes about 10 min to develop, in accordance with Mei et al. (2005). It follows that, for each analyzed wave regime, the viscous steady streaming influences all the tests conducted in the presence of regular waves.

4. Results

4.1. Propagation of the gravity current fronts

The gravity current propagation is here analyzed under different regimes of the ambient fluid, in order to investigate the influence of the waves. In order to describe qualitatively the stages of the propagation of the gravity current front, the onshore front advancement of Test 4 is illustrated in Fig. 4 (g' = 0.13 m/s^2, H = 0.022, T = 0.8 s). The following description is valid for both the onshore and offshore fronts of all the performed experiments. In the first stage, the saltwater fluid is released above the wave surfaces. It is dominated by a vertical transport along the water column (duration 1 ÷ 2 s), with null front horizontal spreading. As the saltwater reaches the channel floor, it propagates radially until it reaches the flume side walls. Such an advancement develops with a nonlinear trend (duration 2.0 ÷ 8.0 s). Such a phenomena recalls the lateral spreading already observed in literature in buoyant low-density plumes (Yuan and Horner-Devine, 2013). Then, the radial expansion stage ends and a close-to two-dimensional front advancement occurs, during which a quasi-linear trend is observed. The present work focuses on the quasi-linear stage of the gravity current propagation.

Fig. 5 shows the advancement of the two fronts, x_{on} in the onshore direction (i.e. positive x) and x_{off} in the offshore direction (i.e. negative x), for all tests. For the sake of the comparison, the front advancement are aligned in order to have the end of the initial collapse stage at a same instant $t^* = t - t_c = 0$, where t^* is the displaced time vector and t_c is the instant when the density current collapse to the bottom.

Comparison between advancement profiles of Fig. 5 show that the front propagation is characterized by an oscillatory behavior with the same period of the wave, as an effect of the superimposed wave motion. This is in accordance with Robinson et al. (2013) and Stancanelli et al. (2017, 2018b). As wave height increases, a slight variation of the front velocities in the onshore and offshore direction, which are calculated as the slope of the quasi-linear phase of the two fronts advancement measured at the bottom of the flume (u_{on} and u_{off}, respectively) is observed for all the experiments. In particular, the differences between u_{on} and u_{off} are not higher than ±0.006 m/s. Moreover, a trend was not identifiable between the different wave and density conditions. Therefore, in contrast to the findings of Robinson et al. (2013), wave motion appears not to significantly influence the front advancement. This is due to the fact that in the present work the gravity current propagation occurs in a density dominated regime. On the contrary, in some of the experiments of Robinson et al. (2013), who tested waves with higher steepness (i.e. H/L up to 0.07), a Stokes-drift dominated regime prevails. The lack of symmetry between the positions of the two fronts observed both in the presence and in the absence of waves is due to the not-perfectly perpendicular spill of the saltwater when it enters the ambient fluid, which cause a shifting of the initial contact point between the denser fluid and the bottom of the channel from x = 0 m (i.e. the abscissas of the release point). Indeed, the differences between the advancements of the two fronts are not compatible with the observed discrepancies between the front velocities during the quasi-linear propagation stage. The shifting of the initial contact point between the denser fluid and the bottom of the channel from x = 0 m is likely to be caused by the initial stage of the entrainment process between saltwater and ambient fluid, which occurs during the gravity current descending phase. Such a shifting is even more evident in

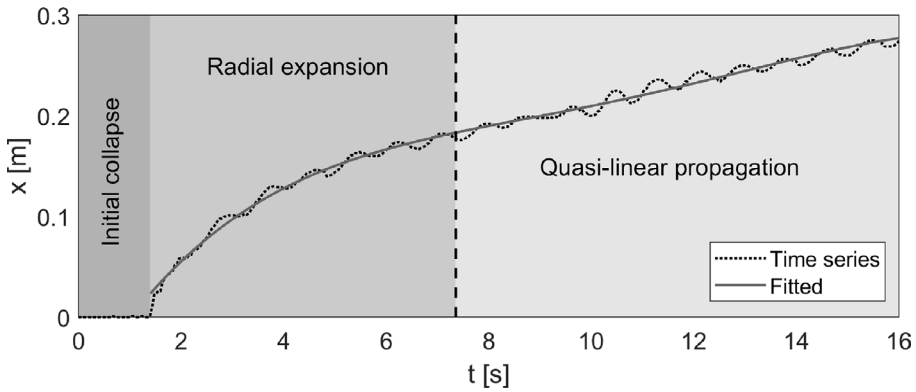

Fig. 4. Stages of the propagation of a point-release front for Test 4 (g' = 0.13 m/s^2, H = 0.022 m, T = 0.8 s), the dashed line represent the instant of the first derivative local minimum.

the presence of waves, because the oscillatory motion enhances the entrainment process.

In order to give an overview on how the density fronts propagate as wave condition changes, Fig. 6 shows the quasi-linear stage front velocities u_{on} (onshore directed, black line) and u_{off} (offshore directed, gray line) as the nonlinearity parameter a/h increases. Since g' did not influence the front advancement velocity, the linear regression of u_{on} and u_{off} as a function of a/h was performed considering tests with different g'. For both onshore and offshore fronts an almost constant trend is observed, with a slight variation of velocity by 0.001 ÷ 0.002 m/s within a wide nonlinearity parameter range (0.03 ÷ 0.07).

4.2. Concentration evolution of the gravity current

The analysis on the density dynamics was carried out in order to study the mixing processes induced by the orbital motion. The construction of concentration maps following the methodology described in Section 2 allows the visualization of the fronts shape and position and of the density distribution in the study area. For the sake of simplicity, Fig. 7 and Fig. 8, shows the concentration maps only for Test 1 (g' = 0.13 m/s^2, no waves) and Test 3 (g' = 0.13 m/s^2, H = 0.022 m, T = 1.0 s), respectively. However, the findings discussed below are valid for all the tested cases. Four different time instants were examined in order to have a framework of the gravity current density evolution in the measuring area, with a time step of 3.00 s. The first instant of each analysis corresponds to the onshore front position x_{on} of about 0.14 m from the release point (i.e. t = 7 s).

For all the tests, the two fronts are characterized by lower density compared to the one observed at the release point. Moreover, the high concentration measured in the core of the gravity current tends to decrease towards the boundary between salt and fresh water. Such phenomena are due to the entrainment process experienced by the saltwater during the descending stage, which leads to a density reduction, as already observed in previous studies, in both lock-exchange (Stancanelli et al., 2018b; Musumeci et al., 2017) and point-release setups Robinson et al. (2013).

The differences between the onshore and offshore fronts at a certain instant can be discussed in terms of shape, concentration spatial distribution and position. Concerning the positions of the two fronts, as already discussed in Section 4.1, they are non-symmetrical for all the tested cases (i.e. both in the absence and in the presence of waves, for all the considered g') because of the shifting of the initial contact point between the denser fluid and the bottom of the channel from x = 0 m.

Fig. 7a shows that in the absences of waves the onshore and offshore fronts are approximately symmetrical, in terms of shape and concentration. Such a symmetry is maintained during the expansion of the gravity current (see Fig. 7b–d). The presence of symmetry of shape between the onshore and offshore fronts can be easily observed by overlapping the outer contour of the gravity current (i.e. the C = 0.15 isoline) at a certain instant with its mirrored copy, after moving the latter of a quantity equal to the shifting of the initial contact point between the saltwater and the bottom of the flume from x = 0 m. Fig. 9a shows the comparison between the outer contours of the onshore and offshore sides of the gravity current for Test 1 at t = 16.00 s. The onshore and offshore fronts are overlapping, with small differences caused by the instabilities at interface between the gravity current and the ambient fluid. The existence of symmetry between the concentration spatial distribution of the two fronts observed in Fig. 7 can be further verified by overlapping the contours of the gravity current corresponding to fixed C-isolines at a certain instant with their mirrored copies, after moving the latter of a quantity equal to shifting of the initial contact point between the saltwater and the bottom of the flume from x = 0 m. Fig. 10 shows the comparison between the contour lines of the onshore and offshore sides of the gravity current for C equal to 0.35, 0.55, 0.75 and 0.85 for Test 1 at t = 16.00 s. The contour lines of the two fronts are always overlapped, thus demonstrating that the concentration spatial distribution of the two fronts is symmetrical.

Fig. 8a shows that in the presence of waves the two fronts initially present a similar shape, but a different vertical distribution of concentration. Indeed, the onshore front is characterized by a more intense mixing between saltwater and ambient fluid with respect to the offshore one, which causes a higher dilution of the saltwater, i.e. a larger low density region. As in the no wave case, the differences between the positions of the onshore and offshore fronts are due to the shifting of the initial contact point between the denser fluid and the bottom of the flume induce by the enhanced entrainement process. The propagation of a portion of the released salt water volume in the offshore direction is observed at the release point, which is consistent with the offshore velocities which characterize the upper part of measured velocity profiles (see Fig. 3).

The differences between the two fronts in terms of shape and concentration distribution becomes more evident during the propagation, as showed in Fig. 8b–d. The onshore front is evidently thinner than the offshore one, which on the contrary is rounded with a thicker mixing region between the gravity current and the fresh water. The absence of shape symmetry between the onshore and offshore fronts is more clearly observed in Fig. 9b, which shows the comparison between the outer contour of the onshore and offshore sides of the gravity current for Test 3 at t = 16.00 s. Moreover, Fig. 11 highlights the lack of symmetry of the concentration spatial distribution of the fronts, by showing the comparison between the contour lines of the onshore and offshore sides of the gravity current for C equal to 0.35, 0.55, 0.75 and 0.85 for Test 1 at t = 16.00 s. The contour lines of the onshore front enclose areas characterized by a thinner shape than the contour lines of the offshore front, thus indicating the lack of symmetry of the concentration spatial distribution.

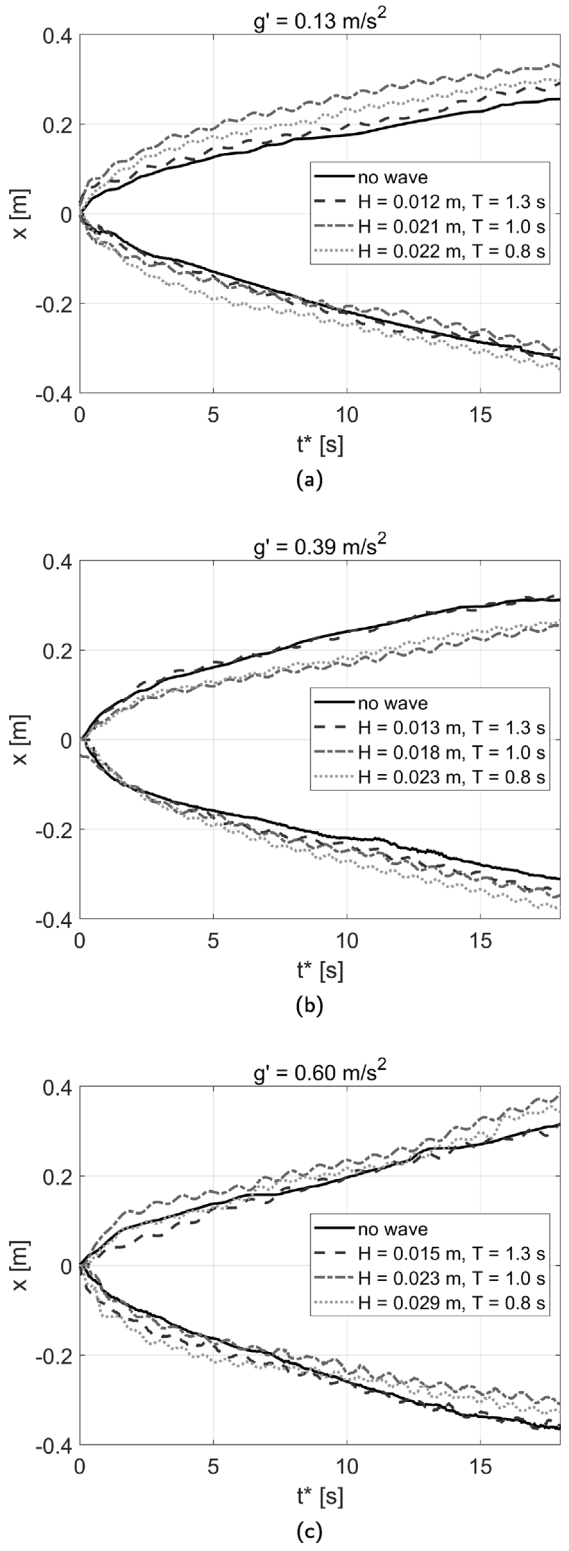

Fig. 5. Front advancement in the onshore direction x_{on} and in the offshore direction x_{off} acquired under different ambient fluid regimes in the case of: g' = 0.13 m/s^2 (Test 1, 2, 3 and 4, subpanel a), g' = 0.39 m/s^2 (Test 5, 6, 7 and 8, subpanel b), g' = 0.60 m/s^2 (Test 9, 10, 11, 12, subpanel c).

The absence of symmetry of shape and concentration spatial distribution, which is in accordance with the findings of Robinson et al. (2013), is a consequence of the velocity profiles showed in Fig. 3. Indeed, the developed steady flow enhances the onshore propagation

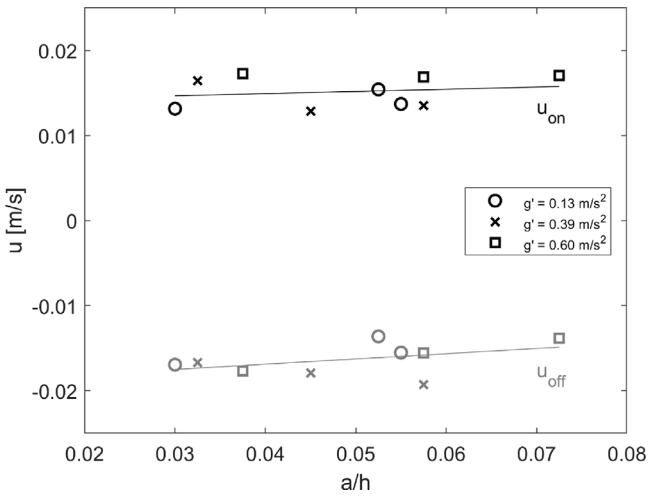

Fig. 6. Dimensionless onshore (black) and offshore (gray) front velocity as nonlinearity increases.

only of the lower part of the density current, thus implicating the generation of a thin front. On the contrary, the negative velocities observed in the higher part of the profile tend to push the upper part of the gravity current towards offshore, thus causing the generation of a thick front, whose rounded shape is due to the wave induced mixing processes. The negative velocities observed in the higher part of the profile also cause the progressive offshore transport of the column of the gravity current collapse. Finally, for all the selected instants, the interface between saltwater and ambient fluid presents more intense 2D turbulent features at the ambient fluid-density current interface in comparison with the no wave tests, due to the interaction between the gravity current and the wave field.

In order to perform a more thorough investigation on the effects of the wave motion on density distribution and mixing phenomena during the quasi-linear progression stage (see Fig. 4, concentration profiles were extracted from the concentration maps for t in the range 12 ÷ 15 s (i.e. in the middle of the quasi-linear propagation stage, see Fig. 4). In particular, the density variation over a wave period was analyzed, to observe how the orbital motion influences the density distribution of the gravity current along the water column, which is represented by the ratio between the z-coordinate and the height of the gravity current (h_{gc}).

The analysis of the concentration vertical profiles in the absence of waves gave similar results for all the tested g'. For the sake of simplicity, Fig. 12 shows only the concentration profiles evaluated for the gravity current with g' = 0.13 m/s^2 in the absence of waves (i.e. Test 1), relative to x = 0.117 m and x = −0.195 (see the reference frame of the concentration maps in Fig. 7 and Fig. 8), which are about 0.100 m behind the onshore and offshore fronts for t equal to 14.12 s. These vertical profiles have been selected in order to investigate the vertical distribution of C of the fronts without being influenced by their non-symmetric position with respect to the release point at x = 0 m (see Section 4.1). The gray shaded area indicates that for z/h_{GC} lower than 0.13 the concentration acquisitions are affected by uncertainties due to the presence of some opacities in the lower part of the glass wall of the flume. Four equally spaced time intervals, namely 14.12 s, 14.42 s, 14.72 s and 15.02 s, were selected to study the concentration profiles over a period whose length is comparable with the tested T (see Table 1). The profiles referred to the four time intervals are almost superposed, for both the onshore and offshore fronts. For the highest z/h_{gc}, greater discrepancies between the profiles can be observed, which are due to the shear stress at the interface between saltwater and ambient fluid. In addition, the onshore and offshore profiles relative to the same t appears quite similar, with slight differences likely due to

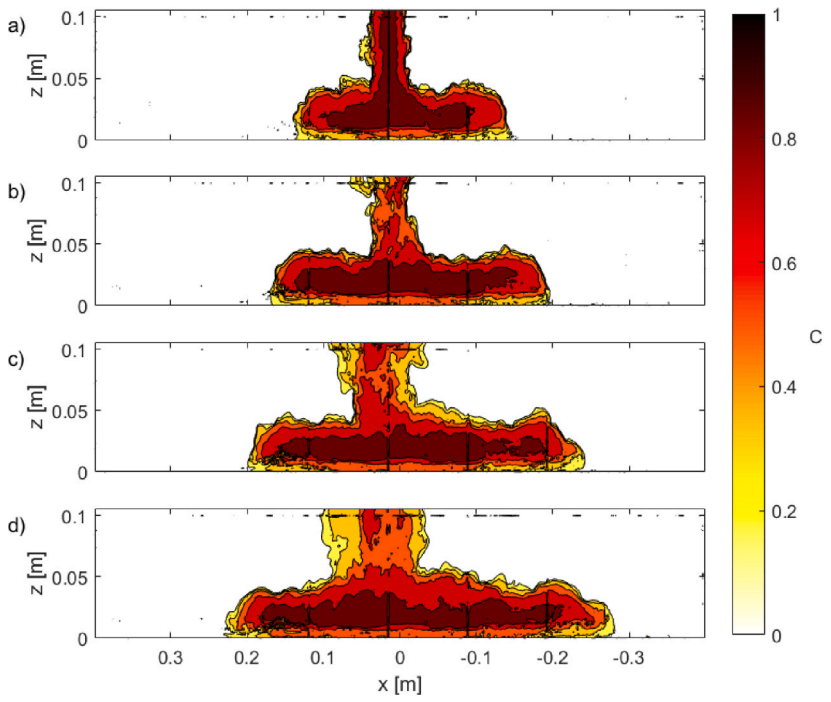

Fig. 7. Concentration maps for Test 1 ($g' = 0.13$ m/s^2 in the absence of waves). The maximum and the minimum value of the concentration represented by the color bar represent respectively ρ_2 and ρ_1. The four panels represent four different instants: 7.00 s (a), 10.00 s (b), 13.00 s (c) and 16.00 s (d) after the start of the test.

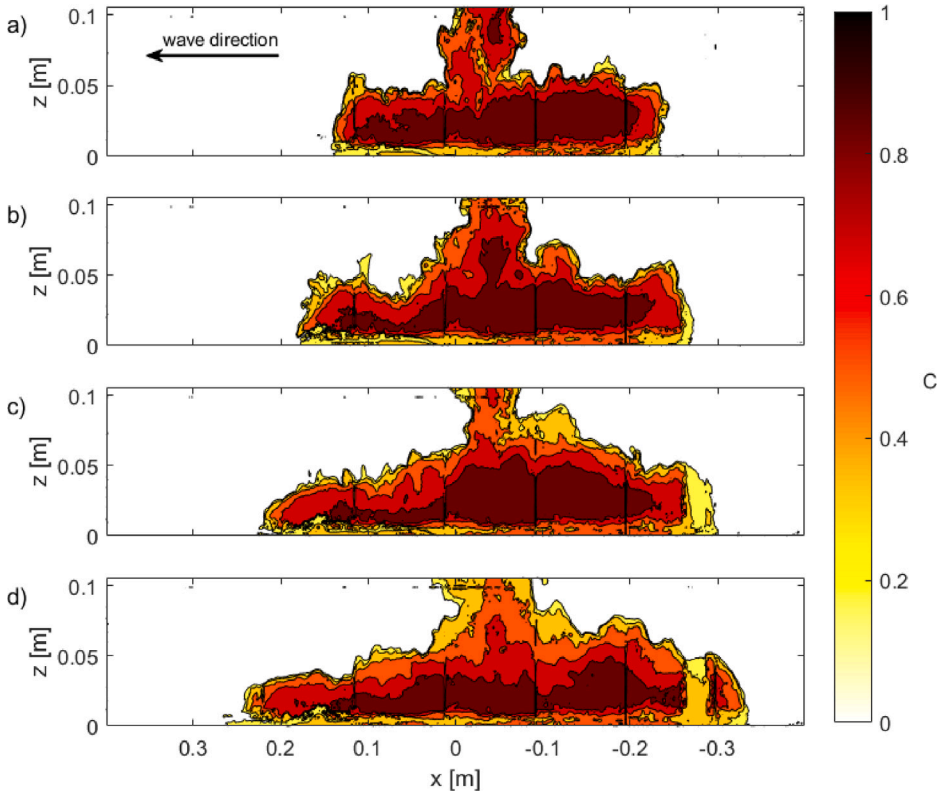

Fig. 8. Concentration maps for Test 3 ($g' = 0.13$ m/s^2, $H = 0.021$ m, $T = 1.0$ s.) The maximum and the minimum value of the concentration represented by the color bar represent respectively ρ_2 and ρ_1. The four panels represent four different instants: 7.00 s (a), 10.00 s (b), 13.00 s (c) and 16.00 s (d) after the start of the test.

the turbulent instabilities along the gravity current interface, as also observed by Robinson et al. (2013).

Fig. 13 shows the concentration profiles evaluated for the gravity current with $g' = 0.13$ m/s^2 (see Figure 13a and c) and $g' = 0.13$ m/s^2 (see Figure 13b and d in the presence of shortest waves i.e. Test 3, Test 4, Test 7 and Test 8). The in-depth investigation of the effects of the longest waves generated during Test 2 and Test 6 on the vertical concentration profiles would require a wider study area. Indeed, in these cases the wavelength is 2.7 times the width of the propagation area. Similarly to the no wave case, the onshore concentration profile

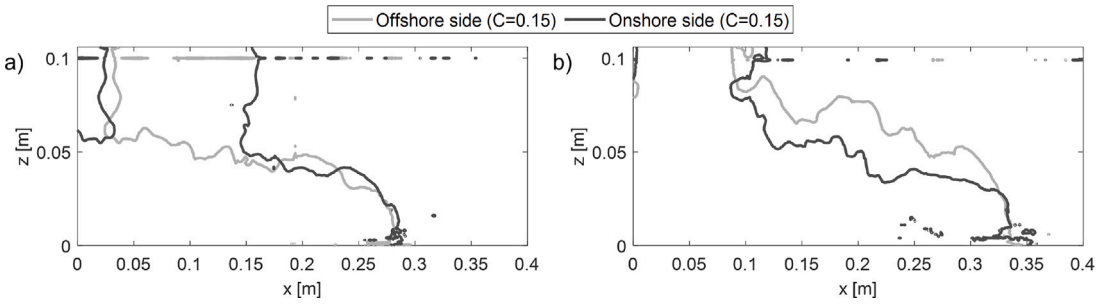

Fig. 9. Outer contours (C= 0.15) of the onshore and offshore sides of the gravity current corresponding to Test 1 (g' = 0.13 m/s^2 in the absence of waves) (a) and Test 3 (g' = 0.13 m/s^2, H = 0.021 m, T =1.0 s) at t=16.00 s (b).

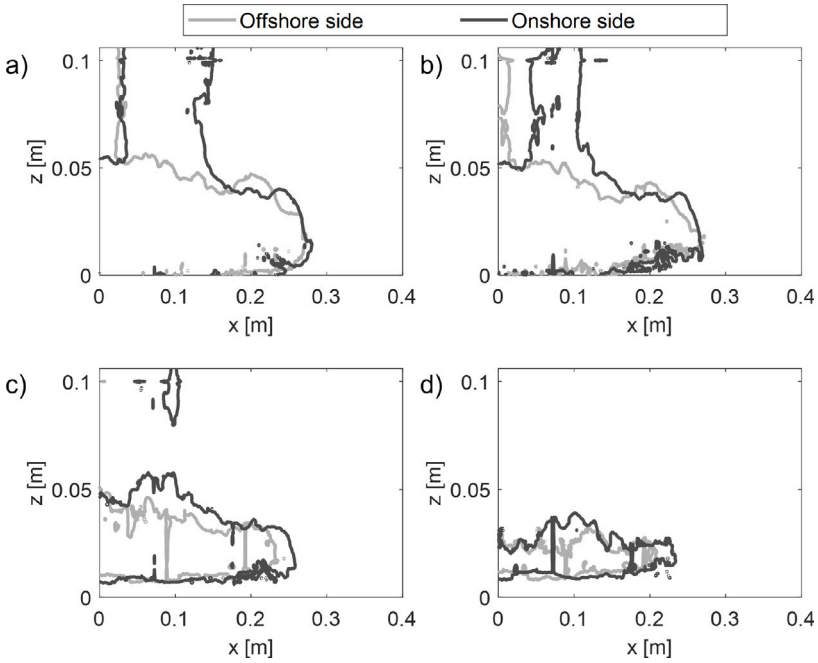

Fig. 10. Contour lines of the onshore and offshore sides of the gravity current for Test 1 at t = 16.00 s (g' = 0.13 m/s^2 in the absence of waves) for C equal to 0.35 (a), 0.55 (b), 0.75 (c) and 0.85 (d).

was extrapolated at x = 0.117 m, which is about 0.100 m behind the onshore front. A time interval between 12 s and 15 s was analyzed, considering the wave zero-up crossing, crest, zero-down crossing and trough phases in x = 0.117 m. The analysis was limited to the onshore vertical concentration profiles, because for the corresponding four offshore vertical concentration profiles, which are distant from the onshore ones by less than one wavelength, the wave phase is undefined.

As the wavelength decreases and the wave height increases, the influence of the wave phase on the concentration vertical distribution is more evident. In particular, the shape of the concentration profiles diverges from the no wave case reaching higher concentrations, to a greater extent for the tests with g' = 0.39 m/s^2. Such a phenomenon is due to the more intense mixing processes produced by the orbital wave motion, which induces a more rapid entrainment of the saltwater from the core of the density current towards the onshore and offshore directions.

The effects of the wave phase on mixing phenomena appears as a piston-type process, which causes lower concentrations when the crest or zero-up crossing phases occur at the selected abscissa. Such a phenomenon is due to the free surface upward oscillation which cause the expansion of the fluid volume. On the contrary, the concentrations along the vertical direction corresponding to the trough and zero-down crossing wave phases are higher, due to the compression effect caused by the lowering of the free surface and the consequent reduction of the water volume. The piston-type process is more evident for the tests with g' = 0.39 m/s^2. Indeed, the latter are characterized by stronger concentration gradients which further enhance the entrainment process occurring between the wave phases. Therefore, the combined effects of wave height and length and g' significantly influence the time variation of the concentration vertical distribution.

5. Summary and conclusions

In the present work the interaction between a two-front gravity current and intermediate water waves was investigated. A series of experiments in a wave flume were conducted, in which the current was generated by means of a point-release setup. The study allowed to qualitatively characterize the dynamics of the current, by identifying three stages of propagation: a first stage of initial collapse of the fluid to the tank bottom, a second stage in which the denser fluid expanded radially with a non-linear advancement, and a third stage of quasi-linear front advancement. The data analysis provided the following results:

- The superposition of the surface waves induces an oscillatory advancement of the gravity current. However the front advancement velocity is not significantly altered by the surface waves as wave amplitude increases, disclosing a density-driven dynamics of the

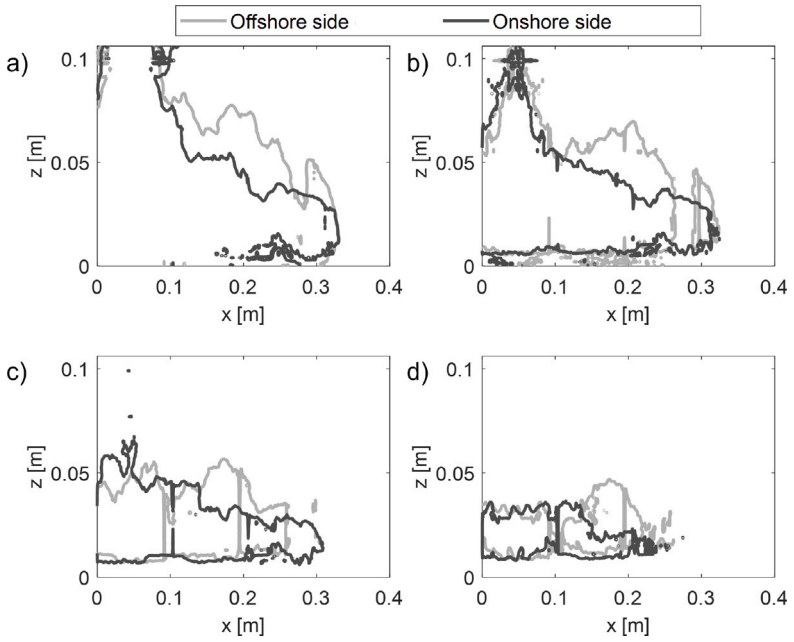

Fig. 11. Contour lines of the onshore and offshore sides of the gravity current for Test 3 at t = 16.00 s (g' = 0.13 m/s^2, H = 0.021 m, T =1.0 s) for C equal to 0.35 (a), 0.55 (b), 0.75 (c) and 0.85 (d).

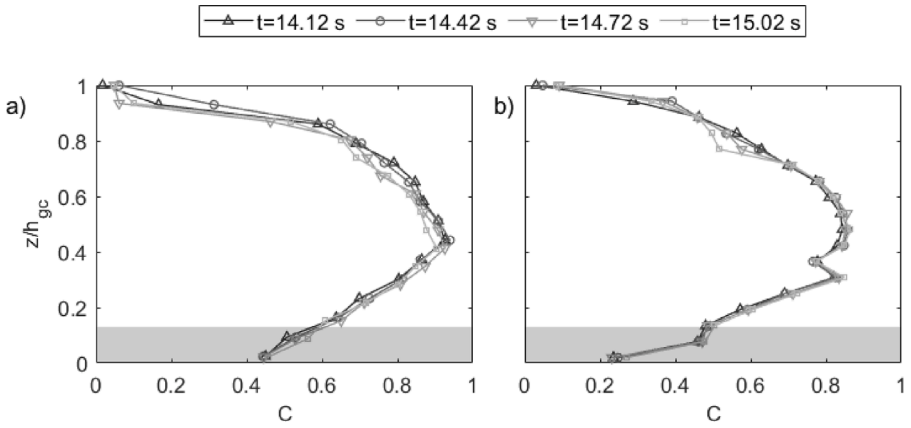

Fig. 12. Dimensionless concentration profiles of the onshore front at x=0.117 m (a) and of the offshore front at x= −0.195 m (b) for Test 1 (g' = 0.13 m/s^2 in absence of waves). The portions of the concentration profiles inside the gray shaded region are affected by some uncertainties due to the limits of the experimental setup.

current for the investigated wave conditions (i.e. intermediate water waves with steepness in the range 0.006 ÷ 0.029).

- The wave motion induces shape and concentration asymmetry between the onshore and offshore current fronts. The onshore front is more angular and thinner than the offshore one, with lower concentrations, as a consequence of the velocity field developed inside the wave flume.
- As wave height increases and the wavelength decreases, a more intense mixing process induced by the orbital motion is observed, which induces a more rapid entrainment of the saltwater from the core of the density current towards the onshore and offshore directions.
- The mixing phenomena is characterized by a ”piston-type” process, which causes for a fixed vertical profile of the gravity current the cyclic decrease and increase of the concentration during the crest and zero-up crossing wave phases, and during the trough and zero-down crossing wave phases respectively.

Our experimental findings show that, for the wave and water depth conditions considered, the presence of waves does not significantly influence the velocity of gravity currents. However, we observed that waves induce an oscillatory modulation in the concentration of the gravity current that can significantly affect the distribution of the denser fluid along the vertical axis. We refer to this phenomenon as a “piston-type” process, which has not been reported in previous investigations and may have fundamental implications, for instance, for marine benthic communities. Specifically, if the gravity current is driven by pollutant transport, the piston-type behavior can impede the vertical dispersion and dilution of the pollutant and lead to higher concentrations at the seabed, exceeding tolerable levels for benthic organisms. Furthermore, the phenomenon can provoke a greater infiltration of pollutants through porous seafloor sediments, expediting contaminant sequestration beneath a porous bed. Alternatively, for a denser current resulting from salinity gradients, the altered salinity levels can cause significant changes in benthic communities, which exhibit a sensitive response to salinity variations that may alter the competitive interactions among the constituent species (Attrill, 2002; Ysebaert and Herman, 2002; Ritter et al., 2005; De Wit, 2011).

Future studies should focus on: (i) extending the wave nonlinearity parameter range in the shallow water direction, in order to investigate effects of larger and more asymmetrical wave velocity fields

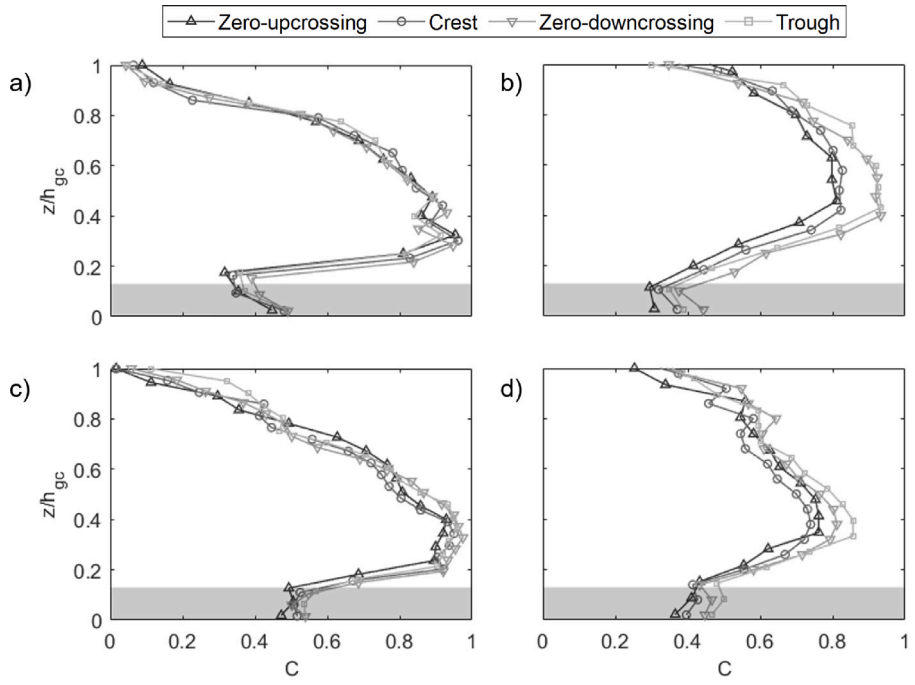

Fig. 13. Dimensionless concentration profiles of the onshore front at x = 0.117 m and: t = 15.4 ÷ 16.1 s for Test 3 (g' = 0.13 m/s^2, H = 0.021 m, T = 1.0 s) (a); t = 12.2 ÷ 12.9 s for Test 7 (g' = 0.39 m/s^2, H = 0.018 m, T = 1.0 s) (b); t = 14.1 ÷ 14.7 s for Test 4 (g' = 0.13 m/s^2, H = 0.022 m, T = 0.8 s) (c); t = 12.3 ÷ 12.9 s for Test 8 (g' = 0.39 m/s^2, H = 0.023 m, T = 0.8 s) (d). The portions of the concentration profiles inside the gray shaded region are affected by some uncertainties due to the limits of the experimental setup.

on the propagation of the current and on the salinity concentration spatial distribution; (ii) reproducing tests with irregular waves to identify similarities between wave motion and fronts propagation spectra; (iii) performing a three-dimensional physical modeling analysis to investigate earlier stages (i.e. radial expansion) of the gravity current generation.

List of symbols

a	Wave amplitude [m]
C	Relative concentration [–]
h	Water depth [m]
h_{gc}	Height of the gravity current [m]
H	Wave height [m]
g	Gravitational acceleration [m/s^2]
g'	Reduced gravity [m/s^2]
L	Wave length [m]
t	Time [s]
t^*	Time with respect to the end of the collapse of the gravity current [s]
t_c	Time when the initial collapse of the gravity current ends [s]
T	Wave period [s]
u	Front velocity of the quasi-linear stage [m/s]
u_{on}	Onshore front velocity of the quasi-linear stage [m/s]
u_{off}	Offshore front velocity of the quasi-linear stage [m/s]
u_s	Stokes drift velocity [m/s]
v_e	Eulerian horizontal velocity between trough and crest [m/s]
V_r	Volume of released dye-saltwater solution [ml]
x	Horizontal coordinate [m]
x_{on}	Onshore front position [m]
x_{off}	Offshore front position [m]
z	Vertical coordinate [m]
δ	Density ratio between a solution of unknown density and a solution of known density [-]
m_2	Weight of the pycnometer with saline solution [g]
m_3	Weight of the pycnometer with distilled water [g]
m_1'	Weight of the empty pycnometer before weighing distilled water [g]
m_1	Weight of the empty pycnometer before weighing saline solution [g]
$\tilde{\rho}$	Fluid density at a generic x and z [kg/m^3]
ρ_1	Saltwater (gravity current) density [kg/m^3]
ρ_2	Freshwater (ambient fluid) density [kg/m^3]

Declaration of competing interest

The authors declare that they have no known competing financial interests or personal relationships that could have appeared to influence the work reported in this paper.

Data availability

Data will be made available on request.

Acknowledgments

This work was funded by the project ”ISYPORT - Integrated System for navigation risk mitigation in PORT” funded under the PNR 2015–2020 program and by the projects ”Interazione Moto Ondoso - Strutture (IMOS)”, REST-COAST - Large scale RESToration of COASTal ecosystems through rivers to sea connectivity (call: H2020-LC-GD-2020; Proposal no. 101037097) and ”VARIO - VAlutazione del Rischio Idraulico in sistemi cOmplessi” of the University of Catania.

References

Adduce, C., Maggi, M.R., De Falco, M.C., 2022. Non-intrusive density measurements in gravity currents interacting with an obstacle. Acta Geophys. 1–12.

Attrill, M.J., 2002. A testable linear model for diversity trends in estuaries. J. Anim. Ecol. 71, 262–269.

Ben Meftah, M., Malcangio, D., De Serio, F., Mossa, M., 2018. Vertical dense jet in flowing current. Environ. Fluid Mech. 18, 75–96.

Bigham, K.T., Rowden, A.A., Leduc, D., Bowden, D.A., 2020. Review and syntheses: Turbidity flows–evidence for effects on deep-sea benthic community productivity is ambiguous but the influence on diversity is clearer. Biogeosciences Discuss. 2020, 1–28.

Cenedese, C., Dalziel, S., 1998. Concentration and depth fields determined by the light transmitted through a dyed solution. In: Proceedings of the 8th International Symposium on Flow Visualization. pp. 1–37.

Chowdhury, M.R., Testik, F.Y., 2014. A review of gravity currents formed by submerged single-port discharges in inland and coastal waters. Environ. Fluid Mech. 14, 265–293.

Cui, T., Kamath, A., Wang, W., Han, D., Bihs, H., 2022. Large-eddy simulations of gravity currents in the presence of waves. J. Hydraul. Res. 60, 770–791.

Dai, A., Huang, Y.L., 2020. Experiments on gravity currents propagating on unbounded uniform slopes. Environ. Fluid Mech. 20, 1637–1662.

Dai, A., Huang, Y.L., 2021. Boussinesq and non-boussinesq gravity currents propagating on unbounded uniform slopes in the deceleration phase. J. Fluid Mech. 917, A23.

De Falco, M.C., Adduce, C., Cuthbertson, A., Negretti, M.E., Laanearu, J., Malcangio, D., Sommeria, J., 2021a. Experimental study of uni-and bi-directional exchange flows in a large-scale rotating trapezoidal channel. Phys. Fluids 33, 036602.

De Falco, M., Adduce, C., Maggi, M., 2021b. Gravity currents interacting with a bottom triangular obstacle and implications on entrainment. Adv. Water Resour. 103967.

De Falco, M., Ottolenghi, L., Adduce, C., 2020. Dynamics of gravity currents flowing up a slope and implications for entrainment. J. Hydraul. Eng. 146, 04020011.

De Wit, R., 2011. Biodiversity of coastal lagoon ecosystems and their vulnerability to global change. Ecosyst. Biodivers. 2, 9–40.

Fannelop, T.K., Waldman, G.D., 1972. Dynamics of oil slicks. AIAA J. 10, 506–510.

Faraci, C., Scandura, P., Foti, E., 2014. Reflection of sea waves by combined caissons. J. Waterw. Port Coast. Ocean Eng. 141, 04014036.

Gonzalez-Juez, E., Meiburg, E., Constantinescu, G., 2009. Gravity currents impinging on bottom-mounted square cylinders: flow fields and associated forces. J. Fluid Mech. 631, 65–102.

Han, D., Xiong, J., Xie, X., Lin, Y., 2021. Effects of emergent and submerged rigid vegetation configurations on gravity current dynamics. Environ. Fluid Mech. 21, 1165–1187.

He, Z., Zhao, L., Hu, P., Yu, C., Lin, Y.T., 2018. Investigations of dynamic behaviors of lock-exchange turbidity currents down a slope based on direct numerical simulation. Adv. Water Resour. 119, 164–177.

Ho, H.C., Lin, Y.T., 2015. Gravity currents over a rigid and emergent vegetated slope. Adv. Water Resour. 76, 72–80.

Kokkinos, A., Prinos, P., 2022. Numerical experiments of partial-depth colliding gravity currents using les. Environ. Fluid Mech. 22, 1081–1105.

Lombardi, V., Adduce, C., Sciortino, G., La Rocca, M., 2015. Gravity currents flowing upslope: Laboratory experiments and shallow-water simulations. Phys. Fluids 27, 016602.

Longo, S., Ungarish, M., Di Federico, V., Chiapponi, L., Petrolo, D., 2018. Gravity currents produced by lock-release: theory and experiments concerning the effect of a free top in non-boussinesq systems. Adv. Water Resour. 121, 456–471.

Maggi, M., Adduce, C., Lane-Serff, G., 2023a. Gravity currents interacting with slopes and overhangs. Adv. Water Resour. 171, 104339.

Maggi, M.R., Adduce, C., Negretti, M.E., 2022. Lock-release gravity currents propagating over roughness elements. Environ. Fluid Mech. 1–20.

Maggi, M.R., Negretti, M.E., Hopfinger, E.J., Adduce, C., 2023b. Turbulence characteristics and mixing properties of gravity currents over complex topography. Phys. Fluids 35, 016607.

Mansard, E.P., Funke, E., 1980. The measurement of incident and reflected spectra using a least squares method. In: Coastal Engineering 1980. pp. 154–172.

Mei, C.C., Stiassnie, M., Yue, D.K.P., 2005. Theory and Applications of Ocean Surface Waves: Nonlinear Aspects. Volume 23. World scientific.

Musumeci, R.E., Viviano, A., Foti, E., 2017. Influence of regular surface waves on the propagation of gravity currents: experimental and numerical modeling. J. Hydraul. Eng. 143, 04017022.

Negretti, M.E., Tucciarone, F.L., Wirth, A., 2021. Intruding gravity currents and re-circulation in a rotating frame: Laboratory experiments. Phys. Fluids 33, 096607.

Ng, C.O., Fu, S.C., 2002. On the propagation of a two-dimensional viscous density current under surface waves. Phys. Fluids 14, 970–984.

Nogueira, H.I., Adduce, C., Alves, E., Franca, M.J., 2013a. Analysis of lock-exchange gravity currents over smooth and rough beds. J. Hydraul. Res. 51, 417–431.

Nogueira, H.I., Adduce, C., Alves, E., Franca, M.J., 2013b. Image analysis technique applied to lock-exchange gravity currents. Meas. Sci. Technol. 24, 047001.

Nogueira, H.I., Adduce, C., Alves, E., Franca, M.J., 2014. Dynamics of the head of gravity currents. Environ. Fluid Mech. 14, 519–540.

Ottolenghi, L., Adduce, C., Inghilesi, R., Armenio, V., Roman, F., 2016. Entrainment and mixing in unsteady gravity currents. J. Hydraul. Res. 54, 541–557.

Parker, G., Garcia, M., Fukushima, Y., Yu, W., 1987. Experiments on turbidity currents over an erodible bed. J. Hydraul. Res. 25, 123–147.

Pelmard, J., Norris, S., Friedrich, H., 2021. Turbulent density transport in the mixing layer of an unsteady gravity current. Adv. Water Resour. 154, 103963.

Ritter, C., Montagna, P.A., Applebaum, S., 2005. Short-term succession dynamics of macrobenthos in a salinity-stressed estuary. J. Exp. Mar. Biol. Ecol. 323, 57–69.

Robinson, T., Eames, I., Simons, R., 2013. Dense gravity currents moving beneath progressive free-surface water waves. J. Fluid Mech. 725, 588–610.

Rottman, J.W., Simpson, J.E., 1983. Gravity currents produced by instantaneous releases of a heavy fluid in a rectangular channel. J. Fluid Mech. 135, 95–110.

Stancanelli, L.M., Musumeci, R.E., Cavallaro, L., Foti, E., 2017. A small scale pressure retarded osmosis power plant: Dynamics of the brackish effluent discharge along the coast. Ocean Eng. 130, 417–428.

Stancanelli, L.M., Musumeci, R.E., Foti, E., 2018a. Computational fluid dynamics for modeling gravity currents in the presence of oscillatory ambient flow. Water 10 (635).

Stancanelli, L.M., Musumeci, R.E., Foti, E., 2018b. Dynamics of gravity currents in the presence of surface waves. J. Geophys. Res.: Oceans 123, 2254–2273. http://dx.doi.org/10.1002/2017JC013273.

Tokyay, T., Constantinescu, G., Meiburg, E., 2014. Lock-exchange gravity currents with a low volume of release propagating over an array of obstacles. J. Geophys. Res.: Oceans 119, 2752–2768.

Venuleo, S., Pokrajac, D., Schleiss, A.J., Franca, M.J., 2019. Continuously-fed gravity currents propagating over a finite porous substrate. Phys. Fluids 31, 126601.

Viviano, A., Musumeci, R.E., Foti, E., 2018. Interaction between waves and gravity currents: description of turbulence in a simple numerical model. Environ. Fluid Mech. 18, 117–148.

Wirth, A., Negretti, M.E., 2022. Intruding gravity currents and their recirculation in a rotating frame: Numerical results. Ocean Model. 173, 101994.

Ysebaert, T., Herman, P.M., 2002. Spatial and temporal variation in benthic macrofauna and relationships with environmental variables in an estuarine, intertidal soft-sediment environment. Mar. Ecol. Prog. Ser. 244, 105–124.

Yuan, Y., Horner-Devine, A.R., 2013. Laboratory investigation of the impact of lateral spreading on buoyancy flux in a river plume. J. Phys. Oceanogr. 43, 2588–2610.